Evaluation of Wing Load Calibration and Sensing Methods Using Conventional Strain Gages and a Fiber Optic Sensing System Installed on a Straight Tapered Wing

Eric J. Miller,[1] Frank Pena,[2] Ashante Jordan,[3] Larry Hudson[4]
NASA Armstrong Flight Research Center, Edwards, California 93523

William Lokos [5]
Jacobs Technology, Inc., NASA Armstrong Flight Research Center, Edwards, California 93523

State-of-the-art instrumentation techniques have provided an opportunity to obtain greater insight into structural wing loads during flight. An investigation was undertaken to research new wing instrumentation and load sensing techniques for measuring accurate in-flight spanwise load distributions on wing structures. A straight tapered wing was instrumented with both conventional foil strain gages at five spanwise wing stations and fiber optic strain sensors at every half inch along the entire wing span. Thirty-nine unique load cases were applied to the wing lower surface using hydraulic actuators to obtain various shear, bending moment, and torque load distributions on the wing. This paper will highlight three load calibration approaches. Conventional linear regression calibration methods were applied to foil strain gages providing a single wing station vertical shear, bending moment, and torque load. Linear regression methods were applied to a fiber optic sensing system to provide bending moment and torque spanwise load distributions. A load sensing scheme using strain derived wing shape information derived from a single load case provided vertical shear and bending moment spanwise load distribution information. Aspects of the three different approaches will be compared and contrasted to inform the reader of the benefits or disadvantages of each. Instrument installation, sensor characteristics, test execution aspects, and recommended calibration techniques will be discussed.

I. Nomenclature

AAW	=	Active Aeroelastic Wing
ACTE	=	Adaptive Compliant Trailing Edge
AFRC	=	Armstrong Flight Research Center
BL	=	butt line
CREW	=	Calibration Research Wing
c	=	distance to neutral axis
d	=	distance
dx	=	difference in *x*
dy	=	difference in *y*
dz	=	difference in *z*
DIC	=	digital image correlation
DOF	=	degrees of freedom
DTF	=	Displacement Transfer Function
E	=	Young's Modulus
EI	=	section properties

[1]Research Engineer, Aerostructures Branch, P.O. Box 273, Edwards, California, 93523, AIAA member.
[2]Research Engineer, Aerostructures Branch, P.O. Box 273, Edwards, California, 93523, AIAA member.
[3]Research Engineer, Aerostructures Branch, P.O. Box 273, Edwards, California, 93523, AIAA non-member.
[4]Research Engineer, Aerostructures Branch, P.O. Box 273, Edwards, California, 93523, AIAA non-member.
[5]Research Engineer, Aerostructures Branch, P.O. Box 273, Edwards, California, 93523, AIAA non-member.

EQDE = equation derivation
ERMS = root mean square error divided by root mean square load
FBG = fiber Bragg gratings
FEM = finite element method
FLL = Flight Loads Laboratory
FOSS = fiber optic sensing system
FS = fuselage station
g = acceleration of gravity
h = structure height at a given cross-section
I = area moment of inertia
ISG = internal strain gage
i = sensor station index number
iFEM = inverse Finite Element Method
j = jth load measurement point
K_{Error} = proportional error
Kp = proportional gain
k = kth strain gage
LAX = lower surface axial gage
LSG = lower surface gage
M = bending moment
m = number of load measurements
NASA = National Aeronautics and Space Administration
n = number of gages
OLEA = Operational Loads Estimation Algorithm
RMS = root mean square
SG = strain gage
UAX = upper surface axial gage
USG = upper surface gage
V = shear load
V_G = initial guess of shear load
V_M = temporary variable for shear load
V_O = shear load output
v = Poisson's ratio
WS = wing station
x_j = measured value
x'_j = derived value
Z = axis aligned in the vertical direction
Z_M = temporary variable for vertical deflection
Z_O = estimated vertical deflection
z = beam displacement
β = strain gage coefficients
ΔL = distance between sensing stations
ε = axial strain
μ = strain gage output
σ = axial stress
ϕ = wing plunge angle relative to horizontal

II. Introduction

Future flight vehicles will incorporate the use of lightweight highly-flexible tailored composite wings and morphing control surfaces. Advances in strain sensing technology have provided the ability to collect strain information along the entire wingspan as compared to only monitoring the strains or loads at a single wingspan station. This paper will highlight the use of a fiber optic sensing system (FOSS) for monitoring the loads on a wing. The results will show the ability to calculate the spanwise load distribution along the wing using FOSS instrumentation methods.

There are multiple reasons one may want to know the loads on a wing in flight, such as airworthiness clearance, health monitoring, structural load alleviation, structural optimization, or aerodynamic model validation. Aircraft

structures have to complete envelope clearance prior to being certified for flight operations. Understanding the loads and verifying that they are staying within limits is critical to accomplishing a successful airworthiness envelope clearance. Multiple projects, such as the Grumman X-29 Forward Swept Wing Research airplane and the F-18 Active Aeroelastic Wing (AAW) (McDonnell Douglas, now The Boeing Company, Chicago, Illinois), flown at National Aeronautics and Space Administration (NASA) Armstrong Flight Research Center (AFRC) (Edwards, California), have all required load monitoring during envelope clearance [1, 2]. Health monitoring schemes also require operational load information over the aircraft lifetime [3]. Having insight into the operational loads environment allows for more informed inspections and maintenance decisions. Structural load alleviation schemes have had some success in the past, but have always been a desired technology for airplane designers. Morphing structures that are now in development, such as the Adaptive Compliant Trailing Edge flown at the AFRC [4], have the ability to shift the load distribution along the wing span to reduce loads during high-g maneuvers or gusts. Monitoring the loads at a high sampling rate and with sufficient accuracy is vital if the control system is required to modify the load distribution during a maneuver or gust. Innovative fabrication techniques such as composite towed steering technology [5] providing new structural optimization capabilities require sensors and monitoring methods that can provide much greater insight into the structural response than conventional sensors located at specific points on a structure. Structural load measurement also can provide insight into the aerodynamic loads. Aerodynamic model validation allows the in-flight measured structural loads with inertial correction to be used to validate computational fluid dynamic and wind-tunnel models. Previous NASA Armstrong projects have called for instrumenting wing surfaces for loads measurements for envelope clearance, but at the same time providing aerodynamic model validation opportunities [6, 7].

Conventional foil strain gages have provided a reliable method for monitoring the vertical shear, bending moment, and torque loads at a few spanwise stations on a wing for many historical airplanes. It is common that only a few spanwise stations are monitored due to the amount of strain gages that are required to be installed. Excessive numbers of strain gages require a great deal of lead wire routing which adds additional weight to the flight vehicle. Available space for internal lead wire routing may also be a limiting factor. Monitoring the loads at a single wing station is usually more than adequate from an airworthiness monitoring and flight envelope expansion standpoint. The X-29 Forward Swept Wing Research airplane which flew at the AFRC during the 1980s was instrumented for airworthiness clearance. The wing instrumentation layout is shown in Fig. 1. The aircraft wing was instrumented with conventional metallic strain gages located on spar caps, webs, and the wing skins. A total of four spanwise stations were instrumented and monitored. Another example, the F-18 AAW, which flew at AFRC in the 1990s, allowed researchers the ability to assess the advantages of using wing torsional flexibility to improve the aircraft maneuverability. The AAW aircraft wings were instrumented at two wing stations, along with a few sensors on the leading and trailing edge control surfaces for load monitoring. The instrumentation layout for the F-18 AAW is shown in Fig. 2. An extensive loads calibration was conducted on the aircraft for calibrating the loads at those spanwise stations. The load pad layout for that test is shown in Fig. 3. The load pad layout allowed the test team to apply various combinations of bending moment and torque loads to the wing.

The purpose of this work was to investigate the use of FOSS to assess whether there is a more expedient and efficient method for obtaining the distributed loads on aircraft structures which allow greater insight into the structural response. The current state of the art sensor platforms now allow designers and researchers a much broader picture of the structural response. In preparation for testing more advanced structures, the Flight Loads Laboratory (FLL), at the NASA AFRC, has conducted the Calibration Research Wing (CREW) test program to load test a moderately flexible General Atomics Aeronautical Systems (Poway, California) MQ-9 wing instrumented with both conventional metallic foil strain gages and FOSS. The test program performed a traditional loads calibration test using conventional strain gages to derive load equations. This industry standard approach was then compared to the results developed from the newer methods using FOSS.

FOSS technology utilizes an optical fiber with fiber Bragg gratings (FBG) distributed along the length of the fiber. The optical fiber is bonded to a substrate or structural surface, and when the substrate is loaded, the fiber senses strain at each FBG location. A typical optical fiber with FBGs with half-inch spacing can make approximately 1000 strain measurements [8]. With this density of strain measurements and the development of new algorithms that effectively use FOSS data, comes the ability to not only measure distributed strains, but also measure distributed shape and loads.

III. Load Sensing Methods

NASA AFRC has an extensive history of flight-testing aircraft structures for real-time load monitoring [9]. With the advent of FOSS technology, it is worthwhile to take a look at the available load sensing algorithms to assess if there are improved methods of load monitoring for aircraft structures. Three load sensing methods will be discussed.

The first is linear regression techniques that have been in use since the 1950s and are the industry standard approach for in-flight load monitoring. Linear regression techniques have been successfully utilized on many structures instrumented with strain gages. Second, this investigation will also take a look at the ability to use FOSS in place of conventional strain gages in a linear regression scheme for calculating the distributed loads on the wing. The third method called the Operational Loads Estimation Algorithm (OLEA) uses strain derived shape information for the structure to back out the distributed shear loads on the structure. This paper documents the first time the OLEA method has been applied to a structure.

In addition to the above methods that will be discussed in this paper, a few additional methods will be highlighted for encompassing the field of load calibration and monitoring methods. Linear regression and OLEA methods are more than sufficient for a simple high aspect ratio wing of this nature. However, low aspect ratio wings with multiple load paths may encounter challenges using these methods. A finite element approach may be more applicable. The inverse Finite Element Method (iFEM) provides an opportunity to measure the loads on the wing when the geometry of the internal structure is known. The iFEM method was developed by Alexander Tessler at NASA Langley Research Center (Hampton, Virginia) over the last 15 years [10-12]. M. Gherlone et al. presented a comprehensive compilation of shape-sensing methods including the iFEM method [13]. The benefit of iFEM is that it does not require material properties or applied loads for calculating the structural shape. The theoretical foundation of the iFEM is minimization of a weighted least-squares smoothing functional that is expressed in terms of the unknown degrees of freedom (DOF) and known elemental strain data.

Once the nodal displacements have been calculated, those displacements can be used to solve for the reaction loads at the boundary conditions by prescribing the displacements onto the FEM nodes. It is possible for the model reaction loads to be solved at any spanwise station. Previous analytical study was conducted using this method and is detailed in Ref. [14]. The study showed that bending moment was matched reasonably well, but shear and torque load matches were not acceptable unless strains from the entire model were used. The iFEM method requires that shear rosettes be installed over the entire structure. This method may be more applicable to a low aspect ratio wing with multiple redundant load paths. The application of this method also potentially eliminates the need to apply load calibration loads to a structure.

It should also be noted that there are additional methods for monitoring loads that do not directly include structural strain information. Correlating wing loads with wing deflections using a multi-linear regression scheme would allow researchers the ability to monitor the wing loads in flight. Lizotte et al, showed the use of a flight deflection measurement system, installed on the AAW aircraft, to estimate the wing bending loads in flight [15]. A similar technique can be used to correlate aircraft state information such as flight measured parameters and control surface deflections, with measured loads to create a loads model. This technique was also used on the AAW project and is discussed by Allen [16]. A similar method discussed by Montel uses a model based approach derived using aircraft state data and pilot inputs to calculate the wing loads in flight [17]. The authors use flight-test data from a UW-9 Sprint (Weller Aircraft Construction, Biberfeld, Germany) to validate their loads model. These methods are shown to highlight other approaches used for load sensing, but will not be discussed in this paper.

A. Linear Regression Method Using Conventional Foil Strain Gages

Calibration of conventional metallic strain gages for loads allows for the monitoring of structural loads in flight. The standard method for calibrating strain gages on a structure makes use of the Skopinski-Aiken Method [18]. The typical loads measured on a wing include shear, bending moment, and torque loads about a measurement station on the wing. Figure 4 highlights the general linear regression scheme with a load station instrumented with conventional strain gages and a load application point outboard of the station. The load point has a corresponding bending arm and torque arm for calculating bending moment and torque loads. The procedure requires collection of applied loads and strain gage data. Loads test points are chosen to vary the center of pressure on the wing surface. Load equations are derived using the applied loads and strain gage output data in a multiple linear regression approach.

Figure 5 shows an example of load data collected during a typical load testing cycle. The linear portion of load cycle three (green arrow) is taken from the dataset for calibration. The first load cycle typically contains hysteresis which is why the third cycle is used in the loads calibration analysis. An example shown in Table 1, shows the vertical shear load, along with the gage output for n, number of gages. Calibrations for bending moment and torque would follow a similar approach as shown for vertical shear load. All the data from the load ramp and all of the load cases total up to make m, the number of load measurements. There may be hundreds or even thousands of load conditions, depending on the sample rate of the data and the number of load cases.

Table 1. Calibration dataset for multiple linear regression for vertical shear.

Load measurement	Applied load	Gage A output	Gage B output	Gage C output	Gage D output	…	Gage n output
1	V_1	$\mu_{1,A}$	$\mu_{1,B}$	$\mu_{1,C}$	$\mu_{1,D}$	…	$\mu_{1,n}$
2	V_2	$\mu_{2,A}$	$\mu_{2,B}$	$\mu_{2,C}$	$\mu_{2,D}$	…	$\mu_{2,n}$
3	V_3	$\mu_{3,A}$	$\mu_{3,B}$	$\mu_{3,C}$	$\mu_{3,D}$	…	$\mu_{3,n}$
…	…	…	…	…	…	…	…
m	V_m	$\mu_{m.A}$	$\mu_{m,B}$	$\mu_{m,C}$	$\mu_{m,D}$	…	$\mu_{m,n}$

A 3-gage equation that uses gages A, C, and D and shear load V can be shown in matrix form in Eq. (1). The least-squares solution for the coefficients β can then be found by Eq. (2).

$$\begin{bmatrix} 1 & \mu_{1,A} & \mu_{1,C} & \mu_{1,D} \\ 1 & \mu_{2,A} & \mu_{2,C} & \mu_{2,D} \\ 1 & \mu_{3,A} & \mu_{3,C} & \mu_{3,D} \\ \cdots & \cdots & \cdots & \cdots \\ 1 & \mu_{m,A} & \mu_{m,C} & \mu_{m,D} \end{bmatrix} \begin{bmatrix} \beta_0 \\ \beta_1 \\ \beta_2 \\ \beta_3 \end{bmatrix} = \begin{bmatrix} V_0 \\ V_1 \\ V_2 \\ \cdots \\ V_m \end{bmatrix} \tag{1}$$

$$[\mu_{j,k}][\beta_k] = [V_j] \tag{2}$$

The AFRC Aerostructures branch utilizes an in-house code referred to as the Equation Derivation Code (EQDE) for deriving the load equations for a single wing station instrumented with conventional strain gages.

B. Linear Regression Method Using FOSS

Not only can conventional metallic strain gages be used in this approach, but the same technique could be used for FOSS. A single FOSS axial sensor or simulated FOSS rosette pattern could be used in lieu of a conventional strain gage and then the linear regression is performed as normal. Figure 4 shows the fiber installations on a wing. FOSS would allow multiple bending moment measurement stations to be designated along the span of the wing. Current computing capabilities permit many multiple linear regressions very quickly and efficiently producing a calibrated set of equations for the distributed load along a wing using FOSS sensors.

C. Operational Loads Estimation Algorithm

The ability to monitor hundreds even thousands of strains has led to the development of shape and load algorithms that take advantage of this new technology. Previous work at AFRC by Dr. Ko et al. [19-21] has shown the benefits of using a displacement transfer function to calculate the deformed shape of a wing under external loading. A large-scale load test of the Global Observer wing (AeroVironment, Monrovia, Califronia) validated the shape algorithms (Jutte et al. [22]). Previous work by Richards and Ko [23] have patented a method for calculating operational loads, but sensor noise can make the method challenging to implement. The Richards and Ko method relies on taking a numerical derivative of bending moments with respect to span to estimate shear load. Though the equations are mathematically correct, measurement noise makes the output less accurate. It is generally advisable to avoid numeric differentiation when possible (Kreyszig [24]), since small inaccuracies in measurements can produce large errors as the length domain converges to a small distance. Another approach by Pak [25], uses the deformed shape from modal testing to calculate the accelerations and velocities which are then are used to calculate the loads on the wing.

This paper describes an algorithm developed at AFRC which allows for the calculation of shear and bending moment distribution along the wingspan utilizing distributed strain measurements to compute wing bending shape and loading information. A brief formulation of the algorithm will be described here. The OLEA, is derived from the Classical Beam Theory (Euler-Bernoulli) for several beam configurations, including cantilever beams which are

analogous with the wing spar structure in an aircraft. The Classical Beam Theory can be used to relate the loading of a structure to the theoretical curvature, slope, and deflection of a cantilever beam. For the purposes of implementing the strain based OLEA, the equation of interest is the moment-strain relationship of the classical beam differential equation which states that the curvature, which is the second derivative of displacement $z(y)$ of a beam, is proportional to the applied bending moment M as shown in Eq. (3):

$$\frac{d^2z(y)}{dy^2} = \frac{M(y)}{E(y)I(y)} \tag{3}$$

Since the bending moment cannot be measured directly, strain sensors placed on the upper and lower surfaces are utilized to quantify the bending moments. The bending stress on the upper surface and the normal stress-strain relationship is expressed as Eq. (4):

$$\sigma_{upper}(y) = \frac{M(y) \cdot c_{upper}(y)}{I(y)} = E(y) \cdot \varepsilon_{upper}(y) \tag{4}$$

where ε_{upper} is the strain measurement on the upper surface, and c_{upper} is the distance to the neutral axis relative to the upper surface. Rearranging terms, it can be shown as Eq. (5):

$$\frac{M(y)}{E(y)I(y)} = \frac{\varepsilon_{upper}(y)}{c_{upper}(y)} \tag{5}$$

As stated by Bakalyar [26], the distance to the neutral axis from the upper surface can be found experimentally by assuming a linear stress/strain distribution from the upper surface (ε_{upper}) to the lower surface (ε_{lower}). A pair of strain gages placed on the upper surface and lower surface at the same span location can be utilized to find the distance to the neutral axis by Eq. (6):

$$c_{upper}(y) = \frac{h(y) \cdot \varepsilon_{upper}(y)}{\varepsilon_{lower}(y) - \varepsilon_{upper}(y)}(y) \tag{6}$$

where h is the height difference between the upper surface sensor and the lower surface sensor. An illustration can be found in Fig. 6. By applying a known load and recording the strain response on the top and bottom surface of the structure, it is then possible to estimate the combined effective section properties (EI). Combining the beam moment equation in Eq. (5) with the neutral axis equation in Eq. (6), the combined effective section properties of the beam structure can be determined by Eq. (7).

$$E(y)I(y) = M(y) \cdot \frac{h(y)}{\varepsilon_{lower}(y) - \varepsilon_{upper}(y)} \tag{7}$$

It should be noted at this point that only one load case is required for obtaining the wing section properties. Once the section properties (EI) have been calibrated, the bending moment for various loading conditions can be estimated by Eq. (8).

$$M(y) = E(y)I(y) \cdot \frac{\varepsilon_{lower}(y) - \varepsilon_{upper}(y)}{h(y)} \tag{8}$$

Numerically integrating the curvature equation in Eq. (3) utilizing the trapezoidal rule, the distributed slope of the structure can be estimated by Eq. (9):

$$\frac{\partial z}{\partial y} = \tan(\phi) \approx \phi_n = \phi_0 + \sum_{i=1}^{n-1} \left(\left(\frac{M}{EI} \right)_i + \left(\frac{M}{EI} \right)_{i+1} \right) \cdot \frac{\Delta L}{2} \tag{9}$$

where *tan* $(\phi) \approx \phi$ for small angles, ϕ_i is the slope angle in the roll orientation at the i_{th} sensing element, with the n_{th} station representing the last sensing station at the tip, ϕ_0 is the root slope, and ΔL is the distance between the sensor stations. The small angle approximation for the tangent function produces a relative error of less than 1 percent for angles less than 10° (0.175 radians), and less than 1-percent error for the sine function with less than 14° (0.244 radians). The small angle approximation also linearizes the relationship between loads and displacement. The vertical displacement (Z_n) at each sensing station can be approximated by integrating the slope equation. The process of determining the vertical displacement at any sensing station n is called the Displacement Transfer Function (DTF) and can be determined by Eq. (10).

$$Z_n = Z_0 + \sum_{i=1}^{n} sin(\phi_i) \cdot \Delta L_i \tag{10}$$

Using small angle approximation sin $\phi \approx \phi$, the calculation for vertical displacement becomes Eq. (11).

$$Z_{OLEA} = Z_0 + \sum_{i=1}^{n} \phi_i \cdot \Delta L_i \tag{11}$$

An illustration of the OLEA flowchart is provided in Fig. 7. The OLEA utilizes the estimated shape (Z_O) from Eq. (11), the calibrated section properties (EI) from eq. (7), and an initial guess of the shear loads $V_G(y)$ as input. The guess shear is then assigned to a temporary shear load variable (V_M) for further processing. The OLEA calculates the shear load by integrating V_M three times with respect to the span to obtain a temporary variable of the distributed span-wise vertical deformation (Z_M). The vertical deflection Z_M is then compared with the estimated shape from the strain based shape (Z_O) and determines the distributed span-wise percentage error between the two (K_{Error}). If the percentage error (K_{Error}) between the two shape estimates is not within desired tolerance, the temporary variable of the shear load (V_M) is updated by multiplying K_{Error} with V_M. A check is applied to the updated shear load variable (V_M) to make sure that the results are consistent with a cantilever configuration, ensuring the shear load at the tip is set to zero, and to ensure that each shear load sensing station ordered from tip to root is greater or equal to the previous sensing station. The updated shear load (V_M) is then reprocessed to obtain an updated Z_M and checked for percentage error. The process repeats in a feedback loop until a desired threshold for K_{Error} is achieved. The shear load variable (V_M) that satisfied the threshold is then processed to provide an output estimate for the applied bending moment M_O and the shear load V_O. For sequentially timed calculations of load, it is recommended that the output results for V_O from the previous time ($time_{i-1}$) frame be fed to the current V_G to reduce the computation time enabling near real-time calculations.

IV. Load Sensing Validation Discussion

The project requirements for load measurement will dictate what the target errors on each load component should be, such as a flight envelope expansion application may be different than an aerodynamic model validation application. A brief survey of past load calibration testing results was conducted so that reasonable expectations could be established for this current investigation. The F-18 errors shown in Table 2 are for a 4-gage load equation that was derived using distributed and point load cases [2]. This case was added mainly to provide additional insight into a past historical example and to show the differences in distributed and point load calibration results. Based on prior load calibration experience, the typical target errors for this wing are expected to be less than 5 percent for vertical shear and bending moment and 20 percent or less for torque loads. Additional load calibration examples can be found in Refs. [9] and [27].

It is important to validate the chosen load sensing method with an independent check case as was done with the F-18 example previously mentioned. A valid check case is one that is not included in the original calibration data set. Typically, a check case is a flight representative case that provides confidence that the load sensing method whether linear regression or a newer method such as OLEA are valid for the expected flight loads. This investigation, just like past efforts calculated the errors between the derived load equations and measured loads taken from an independent check case.

Table 2. F-18 load calibration results.

F-18 load case results – inboard station 4 gage equations, percent		
	Calibration set	Independent check cases
Shear – single point	16	8.5
Shear – distributed	4.5	5.2
Bending – single point	4.5	3.2
Bending – distributed	2.5	2.2
Torque – single point	7.5	5
Torque – distributed	5	5.5

The calculated errors for the derived load equations are obtained by taking the root mean square (RMS) error divided by the root mean square measured load, also referred to as equation root mean square (ERMS), which is a commonly used metric on many previous load calibration tests. The ERMS is shown by Eq. (12). The x_j is the measured value, x'_j is the derived value, and m is the number of load measurements.

$$\text{ERMS} = 100 * \sqrt{\frac{\sum_{j=1}^{m}(x'_j - x_j)^2}{\sum_{j=1}^{m} x_j{}^2}} \tag{12}$$

V. Test Article Description

The CREW test article taken from an MQ-9 is a high aspect ratio composite straight wing with a conventional two spar layout and a half-span of 30 feet. Figure 8 is a photo of the test wing prior to instrumentation installation. The wing contained two trailing edge control surfaces and a fixed leading edge. This wing was an ideal choice for looking at various load monitoring methods due to its simple structure.

VI. Test Article Instrumentation

The test wing was instrumented with conventional foil strain gages, and fiber-optic strain sensors. Deflection potentiometers, inclinometers, and digital image correlation (DIC) targets were also utilized for model validation and test monitoring purposes. Strain gages, in full-bridge configurations, were located at five spanwise stations. Each spanwise station contains eight full-bridge installations on the wing outer surface, as shown in Fig. 9.

Figure 10 shows the locations of the 40 full-bridge strain gage installations at the five spanwise stations on the upper and lower surface. Figure 10 shows the locations of the 14 axial strain gages that were co-located with the fiber optic instrumentation along the forward spar.

Figure 11 shows the locations of the eight internal full-bridge strain gage installations. The internal gages were located at the 4 inboard measurement stations. The most outboard measurement station had no internal strain gages. These gages were located on the spar webs.

The particular FOSS, which was developed at AFRC and licensed to Sensuron (Austin, Texas), can be used to interrogate optical fiber with up to 1,000 distributed FBGs to provide real-time strain data. During structural testing of the wing structure, the FOSS was able to simultaneously and continuously interrogate eight 40-foot optical fibers at 0.5-inch intervals, providing nearly 8,000 strain sensors readings per scan at 20 Hertz.

The FOSS network was installed on the wing in parallel with the coverage provided by the conventional foil strain gages. FOSS generated data were used to calculate distributed wing loading and wing deflections. There were a total of eight fiber runs on the wing with four each on the upper and lower surfaces. Straight fibers run the span of the wing along the forward and aft spars and along the 40-percent chord. A fiber routed in a +/-45 degree saw-tooth pattern runs along the span on the upper and lower surfaces. The saw-tooth patterns create simulated strain rosettes where they meet the straight fiber runs. Figures 12 and 13 show the layout of the fibers on the upper and lower surfaces, respectively. Figure 14 shows a photograph of the completed FOSS installations on the test wing bottom surface.

Documenting the as-installed locations of the FOSS can be a tedious task. The project placed paper targets at specific FOSS locations and then laser scanned the wing. Laser scanning the wing allowed for the project to precisely locate the strain gages and FOSS sensors. Figure 15 shows the laser scanner targets located on the wing. The scanned laser target locations are shown in Fig. 16 along with the FEM model in Fig. 17. This process provided a FEM model that was automatically correlated to the FOSS sensor layout.

VII. Calibration Load Cases

The 39 calibration load cases (load cases 2-40) were broken down into single point and distributed loads. These load cases were designed using engineering experience to move the load center on the wing both inboard and outboard as well as forward and aft. Load case 1 was comprised of 50 lb on each actuator as a holding load to maintain actuator contact with the wing. This case was not considered in the calibration data set and was analytically zeroed for the load calibration analysis. Load cases 2-19 were designated as point load cases, which means only a single hydraulic actuator was applying loads to the wing. Load cases 20-36 were distributed load cases intended for multi-gage load equation derivation. Load cases 37-40 were distributed load cases intended for use as independent check cases for the loads equations derived from load cases 20-36. All of the hydraulic actuators were in contact with the wing during load testing. The actuators that were maintaining contact had a preload of approximately 50 lb. The point loads were converted into shear, bending moment, and torque load based on the load cell load and the moment arms. Figure 18 shows the load cases plotted on a bending moment and torque plot. Figures 19, 20, and 21 show the shear, bending moment, and torque loads, respectively, for the applied load cases.

VIII. Test Setup and Execution

The test wing was cantilevered from a self-reacting wing loads test fixture. The bottom surface of the wing was about 82 inches off of the floor. Four aircraft pins were used to secure the wing spars to a simulated wingbox, which was secured to the test fixture as shown in Fig. 22. Load was applied to the wing using a system of 18 load trains. Each load train included a hydraulic actuator, force transducer, and load pad. The load trains were designed to provide an up load to the wing at 18 load points. Figure 22 shows the deflected wing during test operations.

Eighteen load pads distributed the applied load along both spars on the lower surface. Each load pad had a machined aluminum backing plate with a 0.5-inch thick Neoprene blend closed cell foam rubber bonded to it. The contact surface area for each load pad is 5 inches wide by 20 inches long. Note that the load pads are oriented along the length of the spar. Figure 23 shows the position of the load pads on the lower surface and a picture of a typical load pad. Although all load pads have the same contact area, they are each uniquely contoured for the wing lower surface at the forward and aft spar locations.

IX. Load Sensing Analysis Results

Strain gage, FOSS, and load cell data were collected from load cases 2-40. The data provided a rare opportunity to assess different load sensing methods. Depending on a project's requirements, some of these methods may or may not be pertinent. In this case, the project was able to assess the practicality of linear regression and OLEA shape methods from the given data set. The process for calculating the results will be described along with the results compared against each other. Table 3 highlights the different cases, type of instrumentation, and what calibration and independent check load cases were used.

Table 3. Test result cases.

Method	Calculated loads	Calibration cases	Check cases	Instrumentation
Linear regression	Shear, bending, and torque	Point load cases 2-19	Load case 37 and 40	Strain gage
Linear regression	Shear, bending, and torque	Distributed load cases 20-36	Load case 37 and 40	Strain gage
Linear regression	Bending and torque	Point load cases 2-19	Load case 37 and 40	FOSS
Linear regression	Bending and torque	Distributed load cases 20-36	Load case 37 and 40	FOSS
OLEA – shape method	Shear and bending	Load case 30	Load case 37 and 40	FOSS

The linear regression analysis of the strain gages was accomplished as follows. The data from the load calibration load cases were partitioned into three types: single point, distributed loads, and check cases. The single point load cases 2-19 and the distributed load cases 20-36 were used for multi-gage load equation derivation. Load cases 37-40 are the distributed load cases used as independent check cases for the derived load equations.

The load summation for shear, bending moment, and torsion was created at the 5 spanwise measurement stations for each load case. The data were reviewed to assess the structural hysteresis and signal noise. The third load cycle increasing ramp was used in the derivation. The data were used in the load equation derivation to calculate the strain gage output for all possible load equations for 2, 3, 4, 5, and 6 gages. The load equation derivation is based on a least-squares curve fit. The 4 gage load equations were chosen based on providing reasonable errors for the minimum

number of required gages. The load equation derivation output was compared to the independent check case to create the check case RMS error.

A similar process was used for the linear regression of the FOSS data. Analysis of the FOSS data required load equations to be calculated at every FOSS station (23 total). The number of stations was based on the locations that FOSS simulated shear rosettes were located. The same load cases used for the conventional strain gage linear regression were also used for the FOSS linear regression analysis.

The OLEA shape method analysis used only load case 30 for the calibration case to extract the wing section properties. Load case 30 was the max bending case for the test program. Once the section properties have been calculated, the vertical shear and bending moment loads can be solved for using the OLEA method described above. Using the OLEA method is a simplification to the test execution operation in that only one case is required for the calibration. Given that the test article is a simple high aspect ratio wing, the outboard tip load case is sufficient for obtaining the wing section properties. A low aspect ratio wing may require additional calibration cases.

Load cases 37 and 40 were selected as the independent check cases for assessing the quality of the load predictions. Figures 24 and 25 show the vertical shear load over the wing span for load cases 37 and 40, respectively. The linear regression method using strain gages and the OLEA method was used. The ERMS is also shown for the various methods for both load cases. The shear load plots at first look show reasonably good results. The ERMS comparison for load case 37 show errors of approximately 20 percent, but the larger error is mainly due to taking the difference in derived and measured loads and dividing them by small measured loads. There is a point where low load values and signal noise start to hinder the calculation. The RMS plots will only make comparisons at the 5 span wise measurement stations, all located within the inboard 60 percent of the wing span. The wing inboard section provides a reasonable comparison, less than 5-percent target error, where the signal is above the noise. Load case 40 had larger shear load response than load case 37, thus providing better comparisons over the entire measurement section. Also, the linear regression distributed load calibration had less error than the point load calibration, just as what was found with the F-18 parametric study. The OLEA method was calculated for the shear, and it too matched very well with the truth source. The OLEA match is notable because remember that only one case was required for obtaining the wing section properties.

Figures 26 and 27 show the bending moment comparisons for load cases 37 and 40, respectively. Linear regression calibration was performed using FOSS sensors and strain gages. The OLEA method was performed using only FOSS data. The wing load versus span plots show excellent agreement. The ERMS plots are scaled up to 10 percent to better illustrate differences between the various techniques. The linear regression using FOSS sensors contains slightly more error than the linear regression of the strain gages, and is expected because there were more strain gages available in the loads derivation than FOSS rosettes. It would be expected that with an increase number of FOSS sensors, the FOSS errors would be lower. A majority of the linear regression FOSS sensor errors fall below the target error of 5 percent which compares well to prior tests and is still adequate for most applications. Again the linear regression strain gage distributed load calibration errors are better than the ones derived from the point calibration. The OLEA method bending moment provides errors on the order of linear regression FOSS method.

Figures 28 and 29 show the torque comparisons for load cases 37 and 40, respectively. These plots compare the linear regression of strain gages and FOSS. The target for the torque calibration was 20 percent. Based on prior load calibration tests, the torque error can be much higher. Given the low signal output for load case 37, there are errors larger than the 20-percent target. The linear regression torque results compare better for case 40 than for case 37, and can be explained by observing the strain output for cases 37 and 40. Figure 30 highlights the strains for load case 37 and 40. The shear-strains for check case 37 are lower than case 40 for almost the entire span which explains the poor quality torque comparison for case 37.

The results for check case 37 and 40 compare very well for the linear regression using strain gages and the OLEA method. The results for the linear regression using FOSS data compare qualitatively well to the truth source for the bending moment and torque loads. There are a few things that can be concluded from this short comparison of methods. Linear regression of strain gages provides a reliable method for monitoring loads at individual span stations. The OLEA method works very well for calculating vertical shear loads and provides a sound method for monitoring distributed loads even for low strain outputs such as case 37. The linear regression of FOSS data can work for bending moment and torque load cases as long as acceptable levels of strain are produced. The chord length of the wing did not provide the ability to apply large torque loads. Larger torque load applications would have required applying loads to the control surfaces of the wing or applying loads to the wing using clamping techniques to increase the torsion arm.

A summary of the recommended load sensing methods is shown in Table 4. Overall, conventional strain gages are more applicable to situations which require monitoring a small number of wing stations (5 or less). Anything more than a few wing stations would best be served by FOSS sensors. The sensor locations that have been recommended

for strain gages are still applicable to FOSS sensors. FOSS may be easier to install on the wing surface compared to a spar web and may require the OLEA method instead of possibly using linear regression techniques. Linear regression methods are still preferred for bending moment and torque calculation due the ease of implementation. Unless FOSS simulated shear rosettes are installed on the shear web, or a large number of conventional shear strain gage rosettes, the OLEA method will need to be used. FOSS and OLEA provide the ability to measure shear loads using a single calibration load case. The reader should be careful using only one load case for linear regression methods. The only time using one calibration case is possible is for structures with straightforward load paths when calculating bending moments. Table 4 summarizes the available approaches for load calibration of a high aspect ratio wing using strain gages or FOSS.

Table 4. Load sensing recommendations for a high aspect ratio wing.

Load type	Recommended sensor	Strain sensor orientation and location	Recommended number of load cases	Recommended calibration method
Shear – single wing station	Conventional strain gages	Shear rosette located on shear web Axial strain sensor located on spar caps	Number of load cases > number of strain sensors in the equation	Linear regression
Bending moment – single wing station	Conventional strain gages	Axial strain sensor located on spar caps	1 load case	Linear regression
Torque – single wing station	Conventional strain gages	Axial strain sensor located on spar caps Shear rosette located on shear web or skins	Number of load cases > number of strain sensors in the equation	Linear regression
Shear – distributed load	FOSS sensors	Axial strain sensor located on spar caps	1 load case	OLEA
Bending moment – distributed load	FOSS sensors	Axial strain sensor located on spar caps	1 load case	Linear regression
Torque – distributed load	FOSS sensors	Axial strain sensor located on spar caps Shear rosette located on shear web or skins	Number of load cases > number of strain sensors in the equation	Linear regression

X. Instrumentation Trade Study Discussion

The ability to measure thousands of strains with a fiber the diameter of a hair has many benefits for the aerospace field [8]. The advantages and disadvantages of fiber and strain gages will now be discussed. Metallic foil strain gages have been around for many decades, and the installation and monitoring processes are well known. A strain gage full bridge has self-temperature compensation. A strain gage rosette can be installed easily to monitor high stress areas or in hard to reach places where a single measurement is required. A requirement for only a small number of strain sensors are most likely best handled by strain gages. In comparison, fiber optics are more for open areas that require a large number of sensors like a wing skin or even a spar web. Fiber can be routed in such ways to create strain rosettes similar to that of rosette strain gages. There are numerous benefits to installing fiber. Fiber has the capability to be multiplexed serially allowing for multiple spanwise measurements on one fiber. Fiber is lightweight for the number of strain sensors available compared to the weight of a similar number of strain gages. FOSS is also immune to electro-magnetic interference or electro-magnetic pulses unlike strain gages. Given a large number of sensors, fiber can be installed much quicker than an equal number of strain gages. The monitoring objectives for a project will determine the ideal sensor whether it be FOSS or conventional strain gages.

XI. Conclusions

A straight tapered wing was instrumented with conventional foil strain gages and fiber optic strain sensors. This paper showed the results of using conventional linear regression calibration techniques and a wing shape algorithm to calculate the distributed vertical shear, bending moment, and torque loads along the wingspan. This paper was a first

step in characterizing the different approaches. The project requirements for load monitoring play a key role in determining which sensor and load sensing method should be used whether it be for airworthiness envelope clearance, structural health monitoring, load alleviation, structural design optimization, or aerodynamic model validation.

The five strain gage instrumented spanwise stations were calibrated using linear regression techniques for shear, bending moment, and torque loads utilizing approximately 20 load cases. The advantages to using conventional metallic strain gages and linear regression techniques are the fact that it is a straight forward, efficient method for monitoring loads on a wing for airworthiness flight clearance. The disadvantage is that only a small number of wing stations can be monitored, and a large number of load cases are required for the calibration. Additional sensing stations increase the wire weight and routing complexity. The arrival of FOSS installed on the outer wing surface in conjunction with the use of linear regression techniques can be used to calculate a distributed bending and torque load along the wing. The test results plotted in this paper show that linear regression techniques for FOSS can work. The wire weight and routing complexity issues are then greatly reduced.

The OLEA shape method provided a very good match to the check cases for shear and bending loads and was similar to a conventional calibration using conventional metallic strain gages and linear regression techniques. Using the state of the art FOSS approach, only a single load case was required to calibrate the system to provide the distributed loads over the wing span, thus providing a great deal more load information for flight monitoring. Strain gages would not have been applicable for this method. The results of this study clearly demonstrate that there are advantages to be gained by using FOSS instrumentation in terms of providing distributed wing load information, reducing instrumentation weight, and reducing load test calibration complexity.

Figures

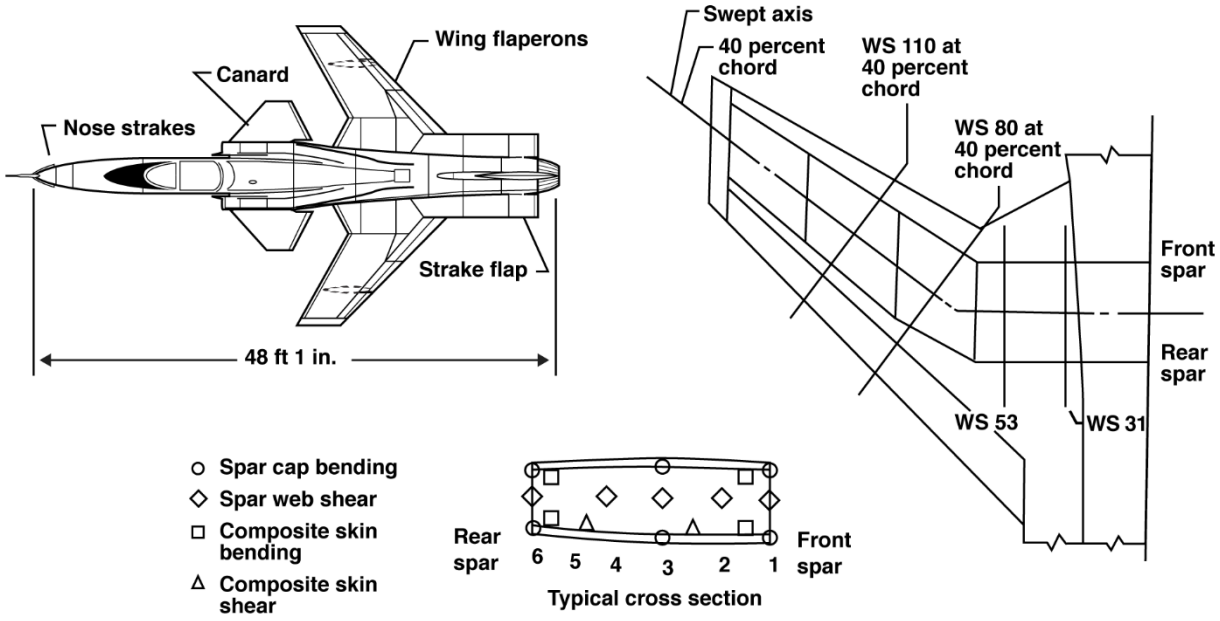

Fig. 1. X-29A forward swept wing load measurements.

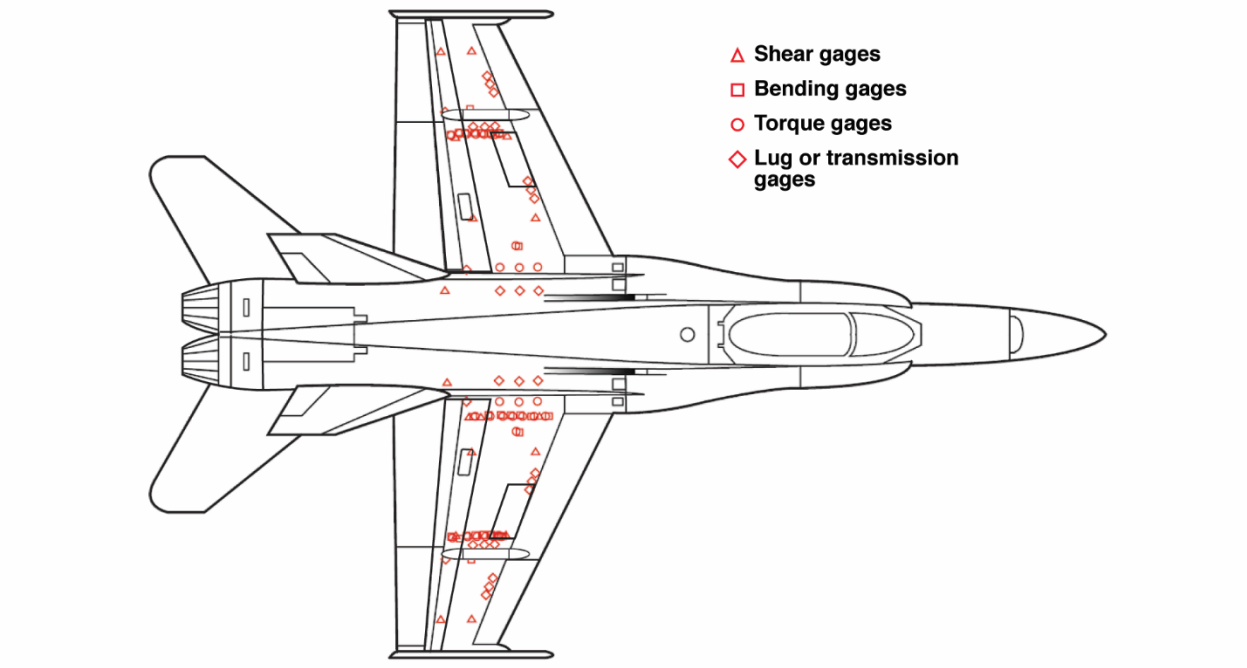

Fig. 2. Active Aeroelastic Wing load measurements.

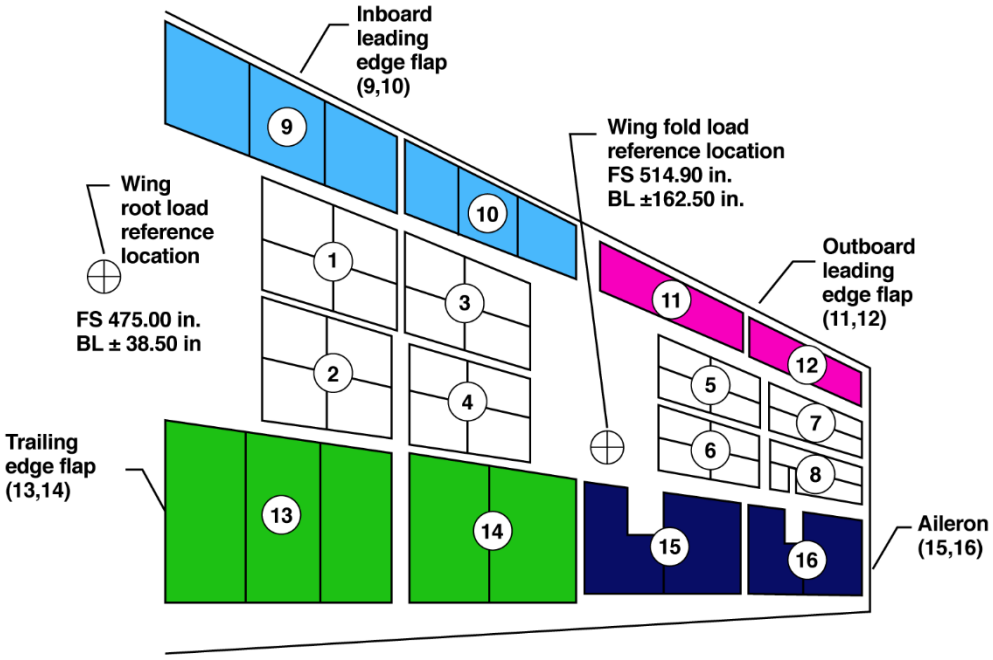

Fig. 3. Active Aeroelastic Wing loading zones.

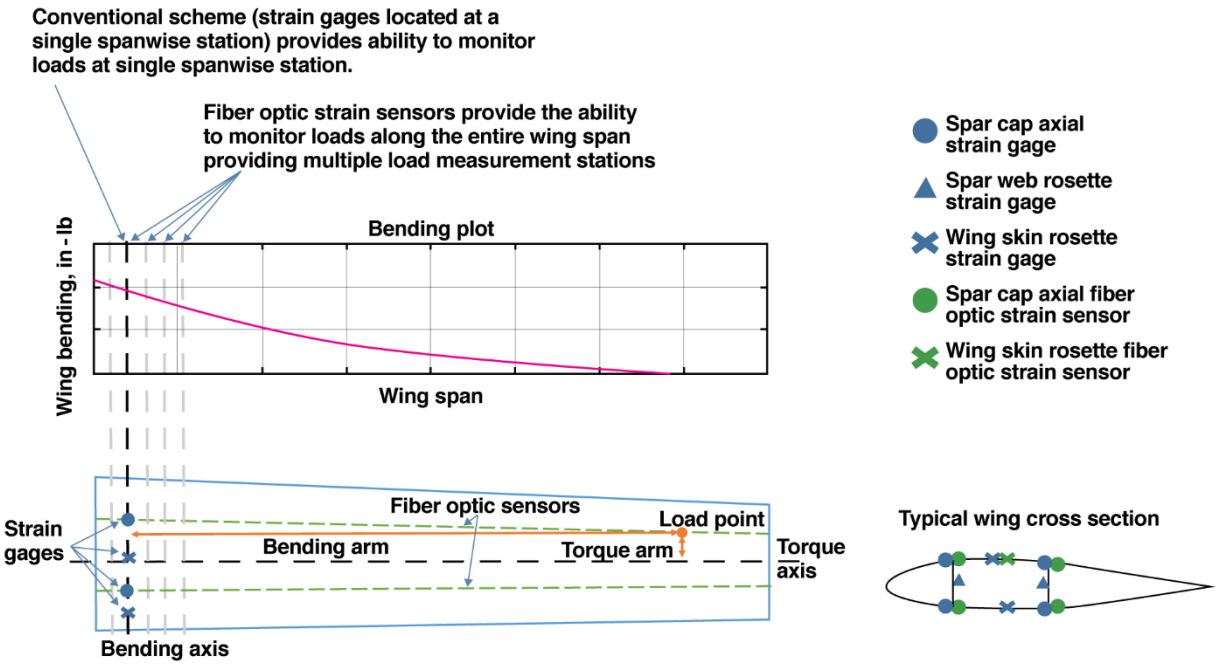

Fig. 4. Wing load description.

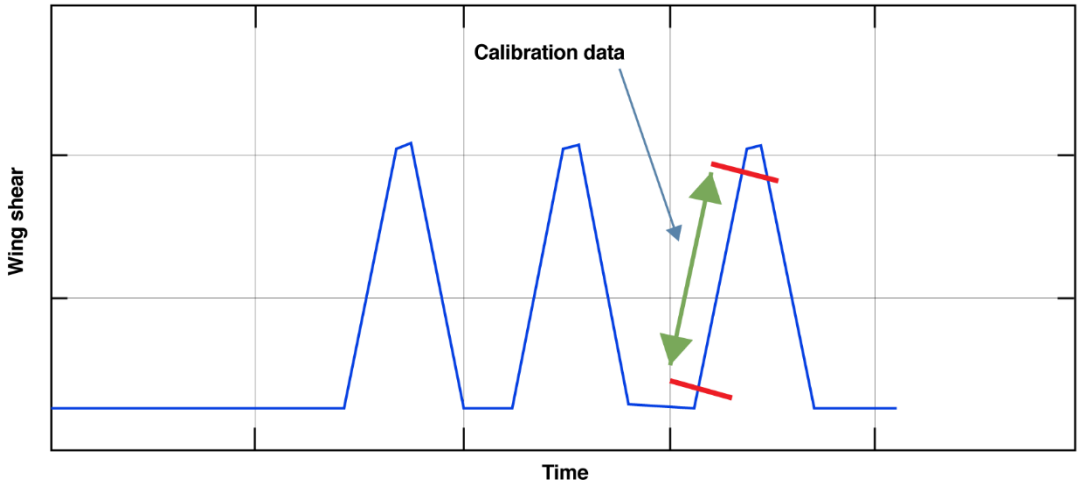

Fig. 5. Data for loads calibration.

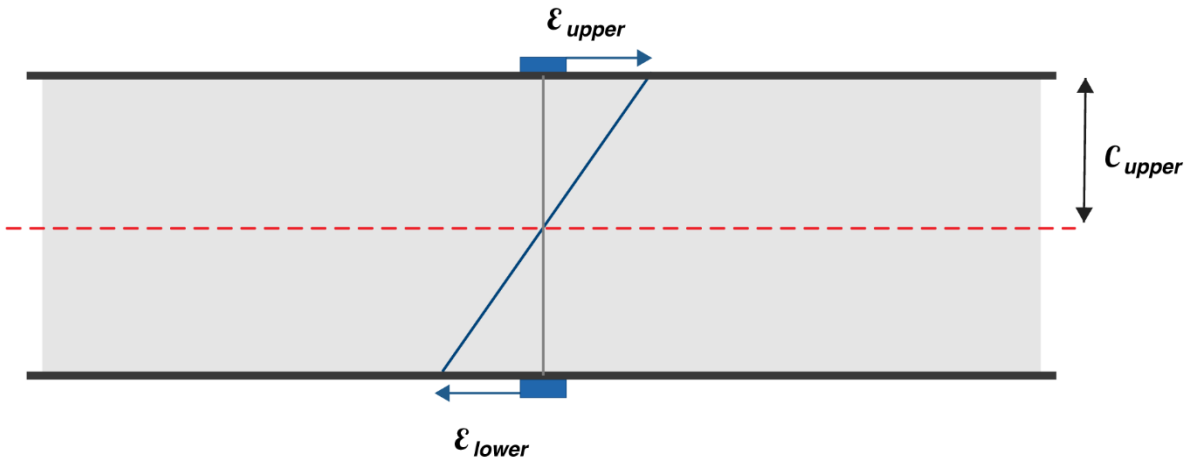

Fig. 6. Strain description for Operational Load Estimation Algorithm.

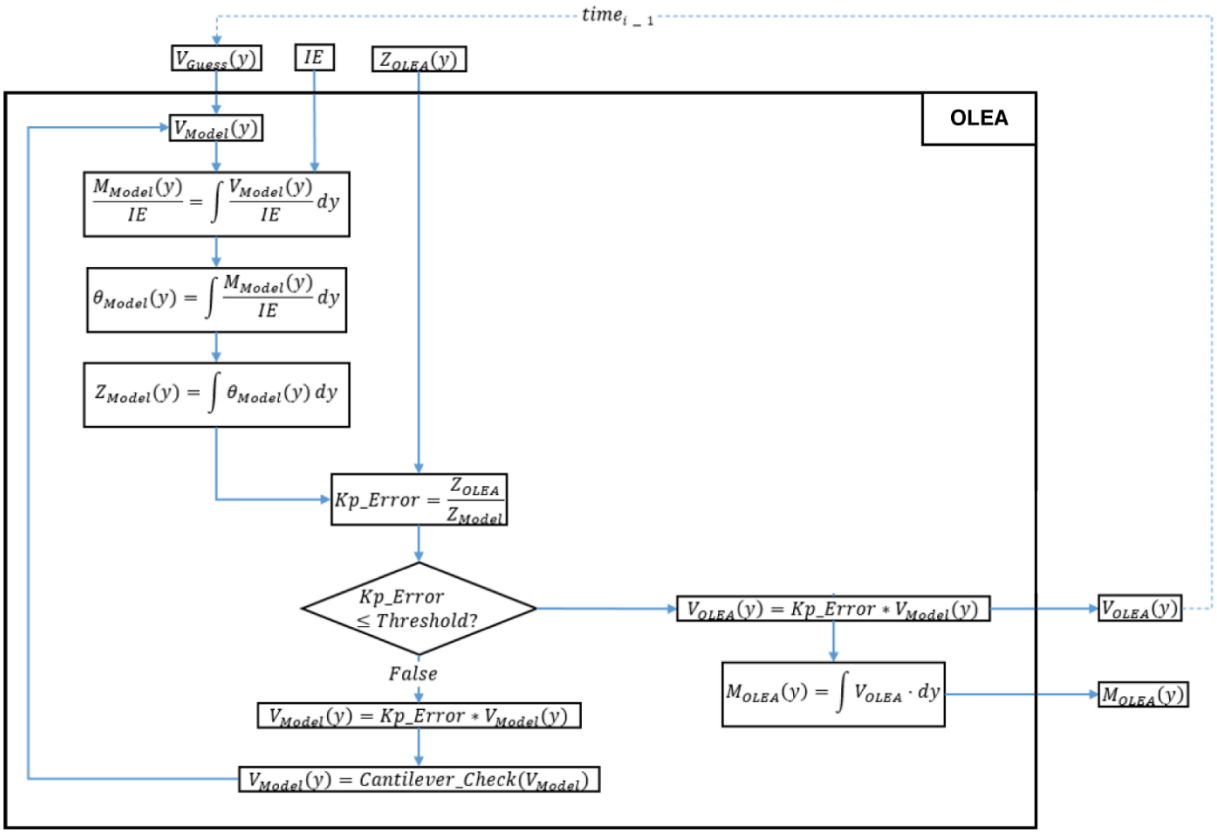

Fig. 7. Operational Load Estimation Algorithm flowchart.

Fig. 8. Wing test article.

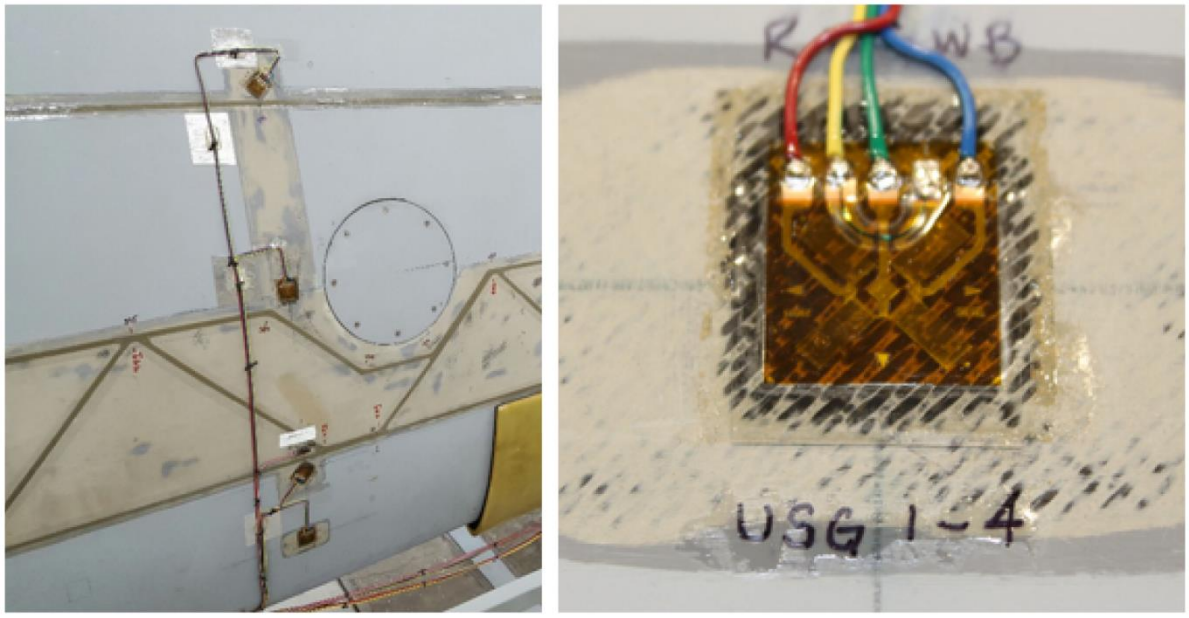

Fig. 9. Strain gage installations at a typical spanwise station.

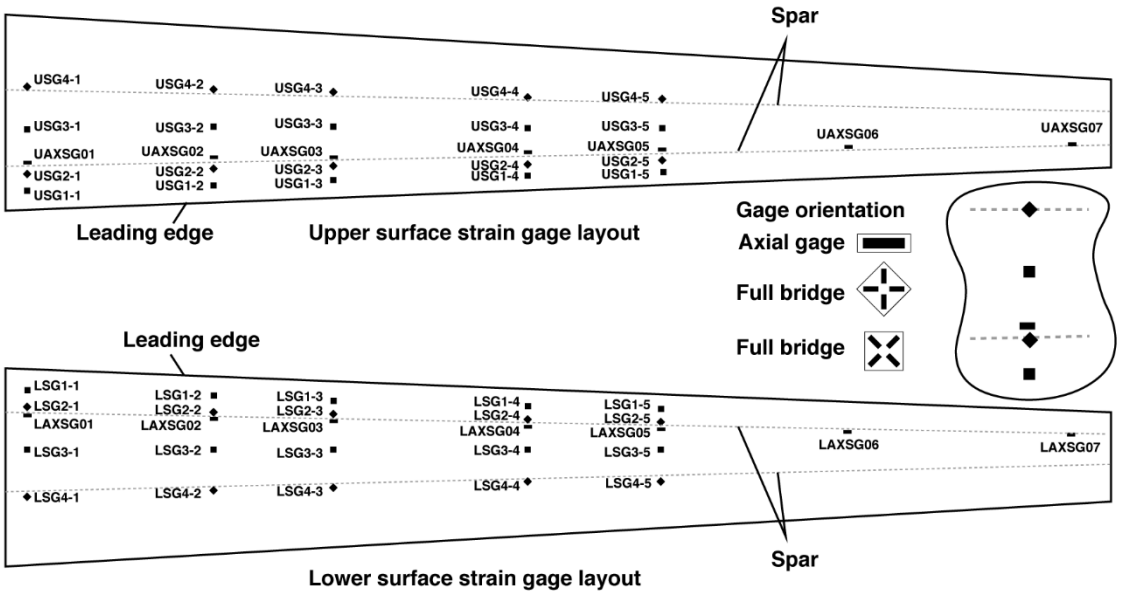

Fig. 10. Strain gage instrumentation on upper and lower surfaces.

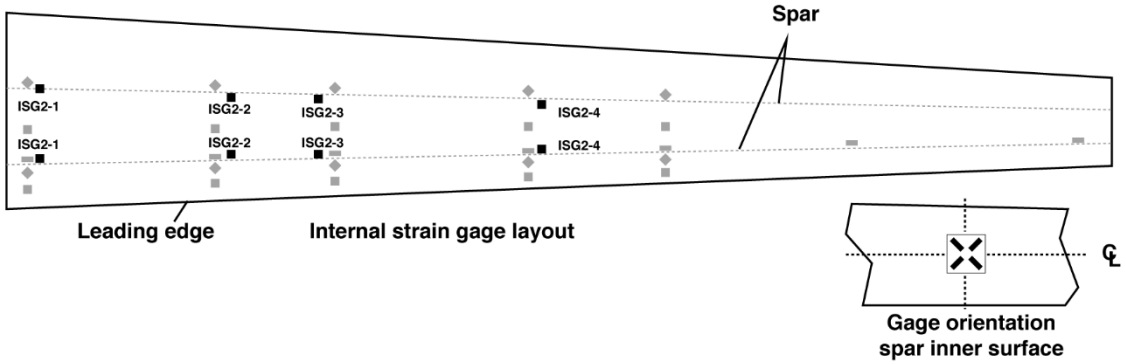

Fig. 11. Internal strain gage locations.

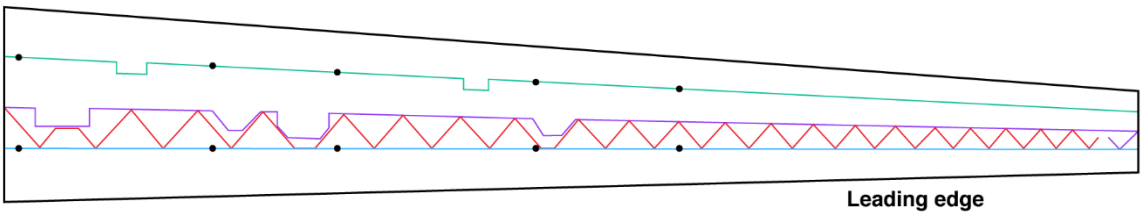

Fig. 12. FOSS layout on upper wing surface.

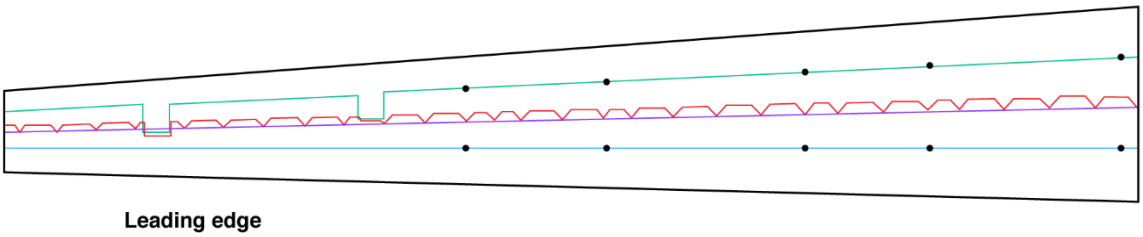

Fig. 13. FOSS layout on lower wing surface.

Fig. 14. Completed FOSS installation.

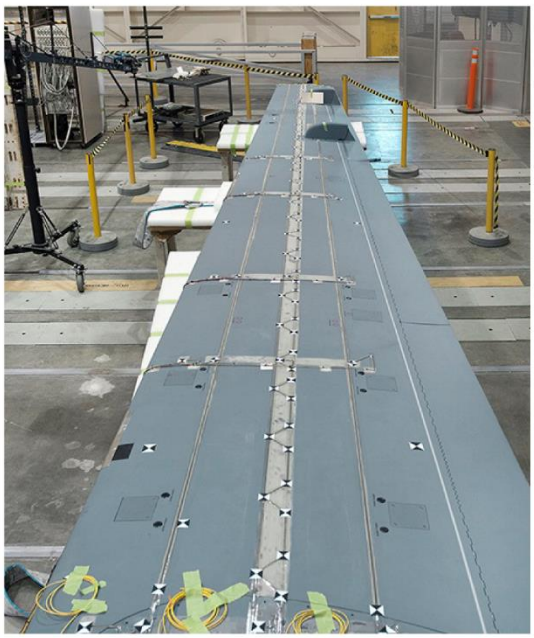

Fig. 15. Laser scan target locations.

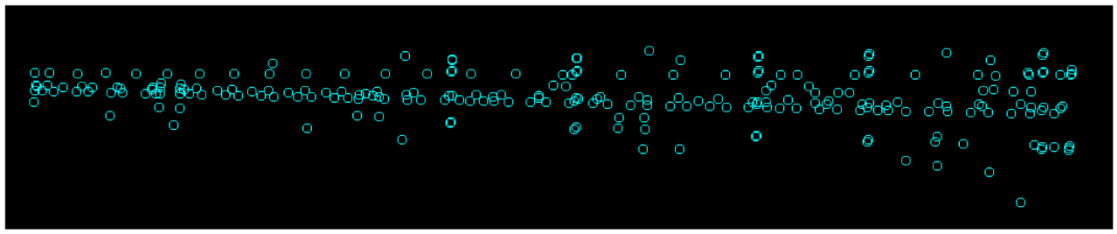

Fig. 16. Laser scanned targets.

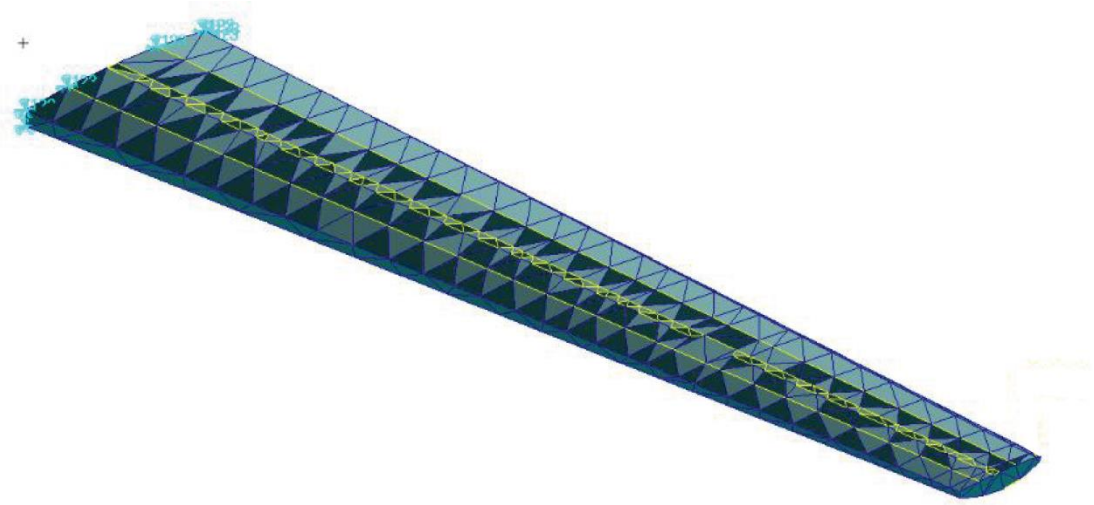

Fig. 17. FEM model created from laser scan.

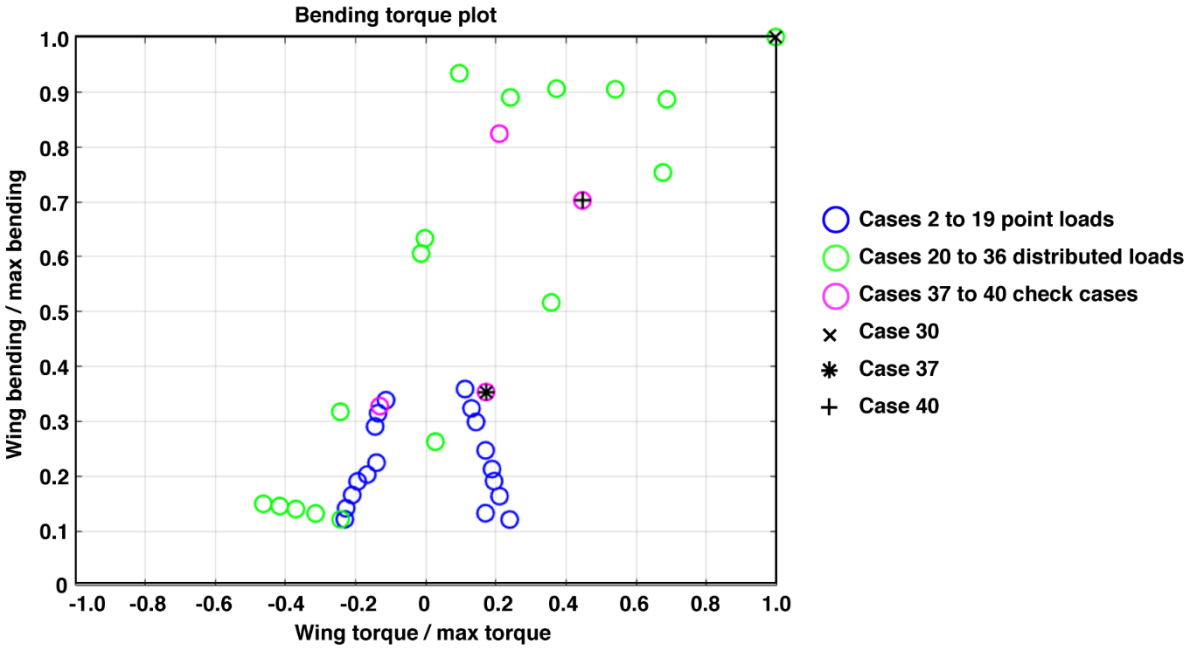

Fig. 18. Bending torque plot.

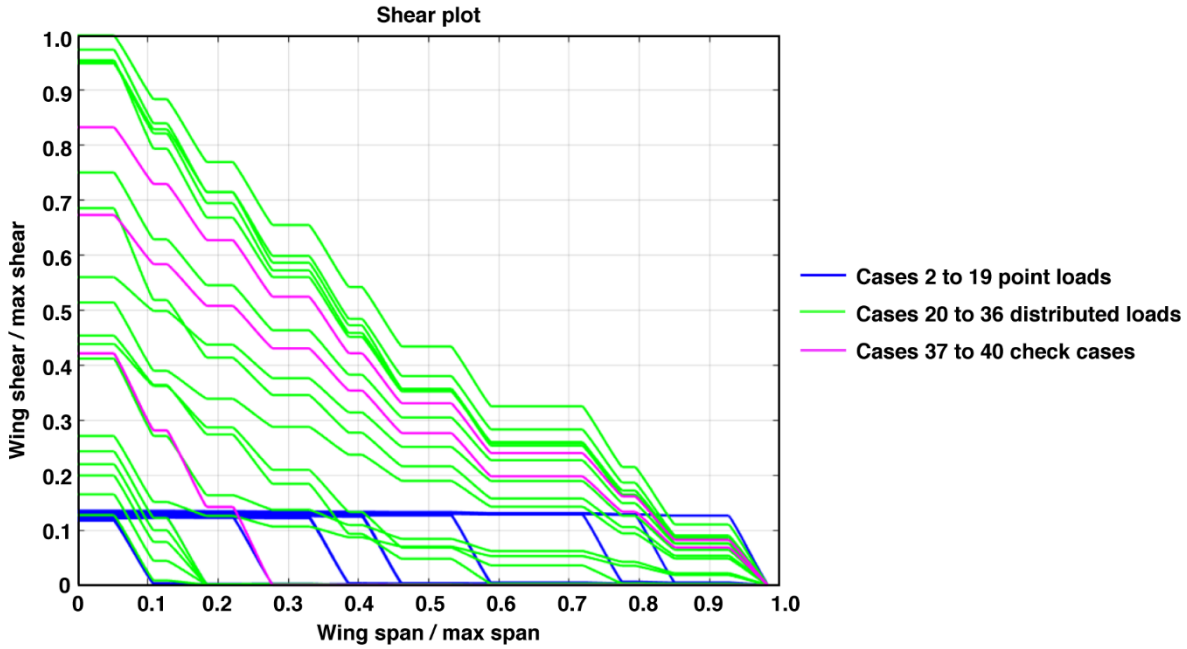

Fig. 19. Load cases – shear loads.

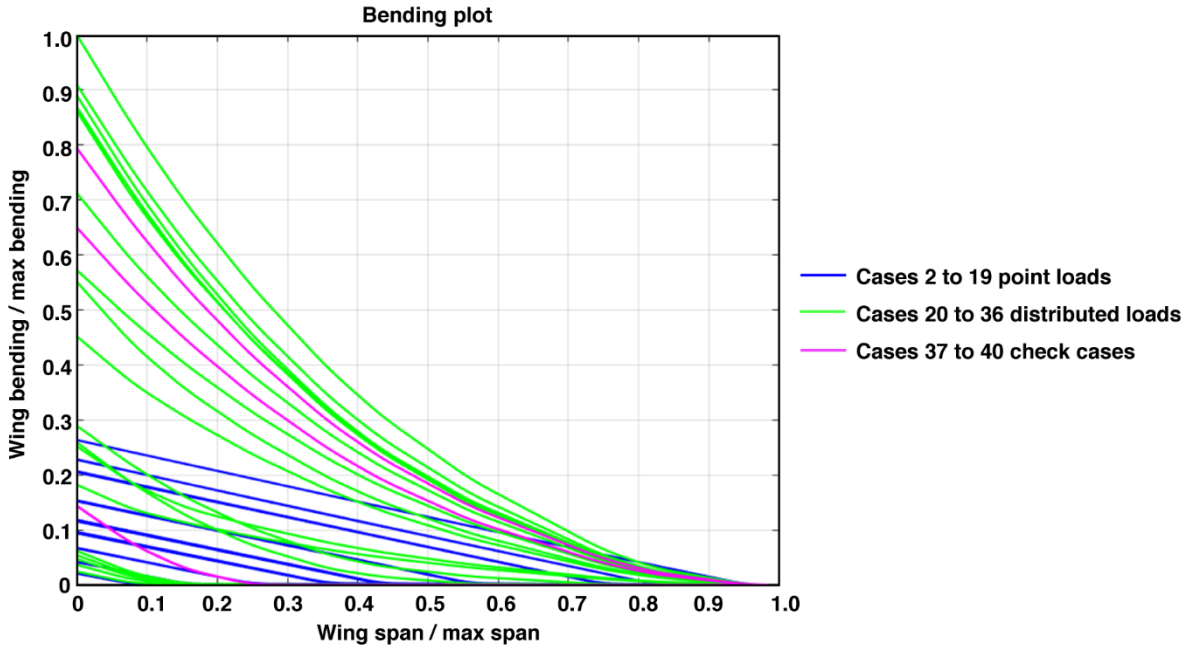

Fig. 20. Load cases – bending loads.

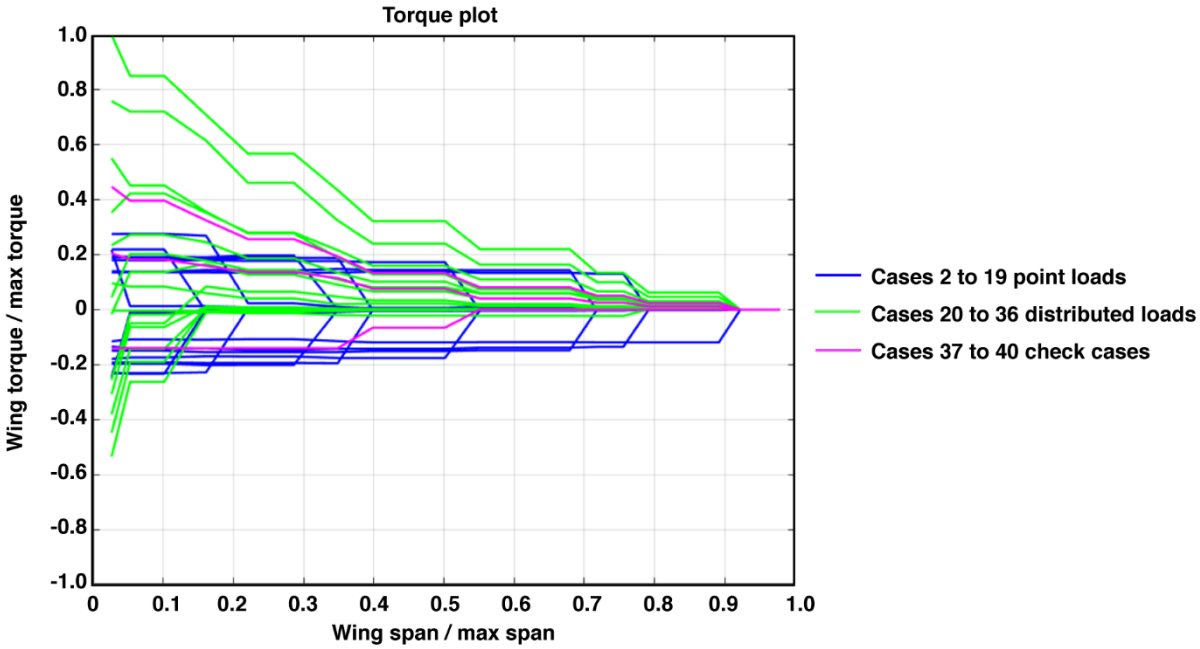

Fig. 21. Load cases – torque loads.

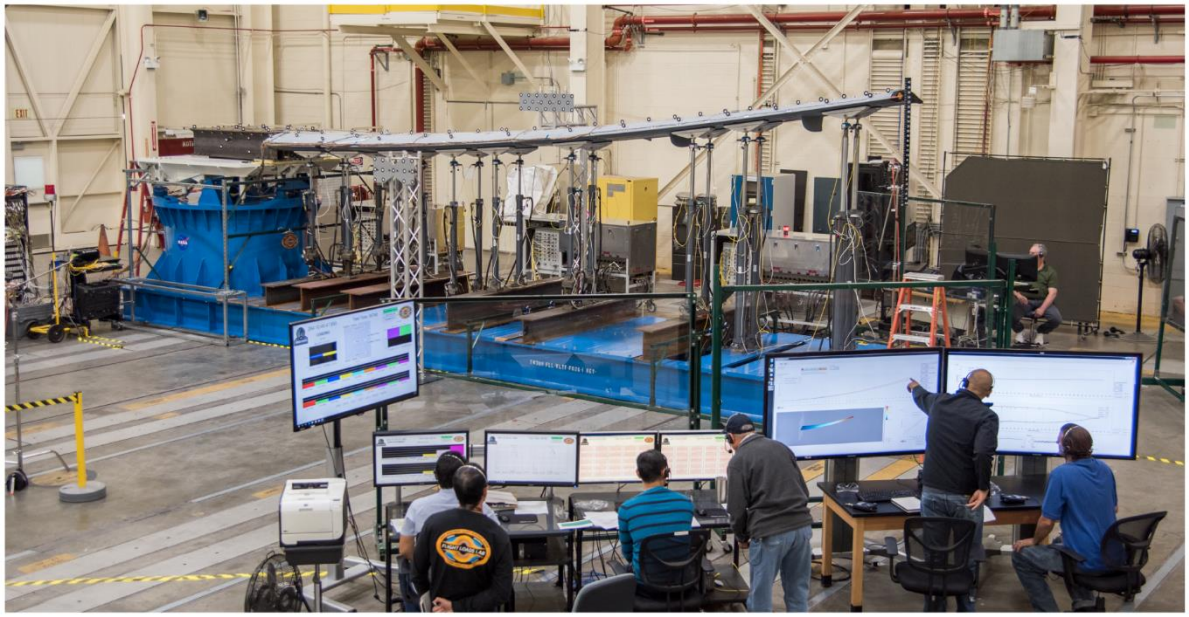

Fig. 22. Test execution.

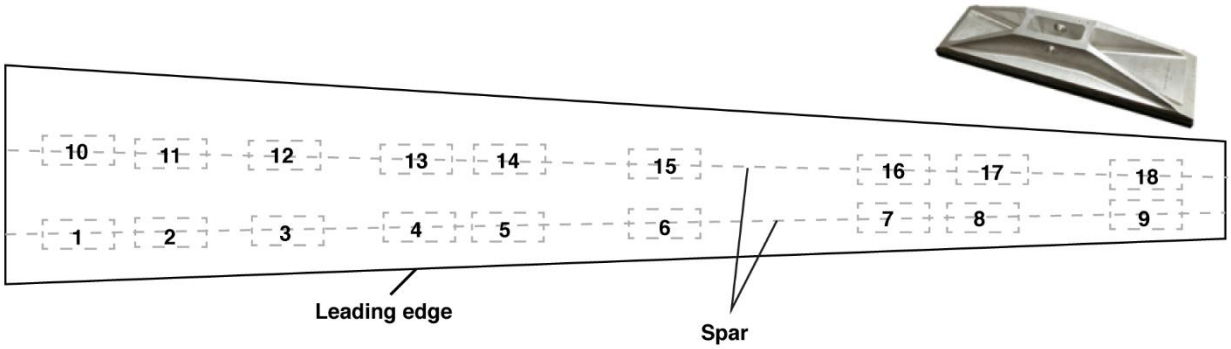

Fig. 23. Load pad locations and loading zone numbering.

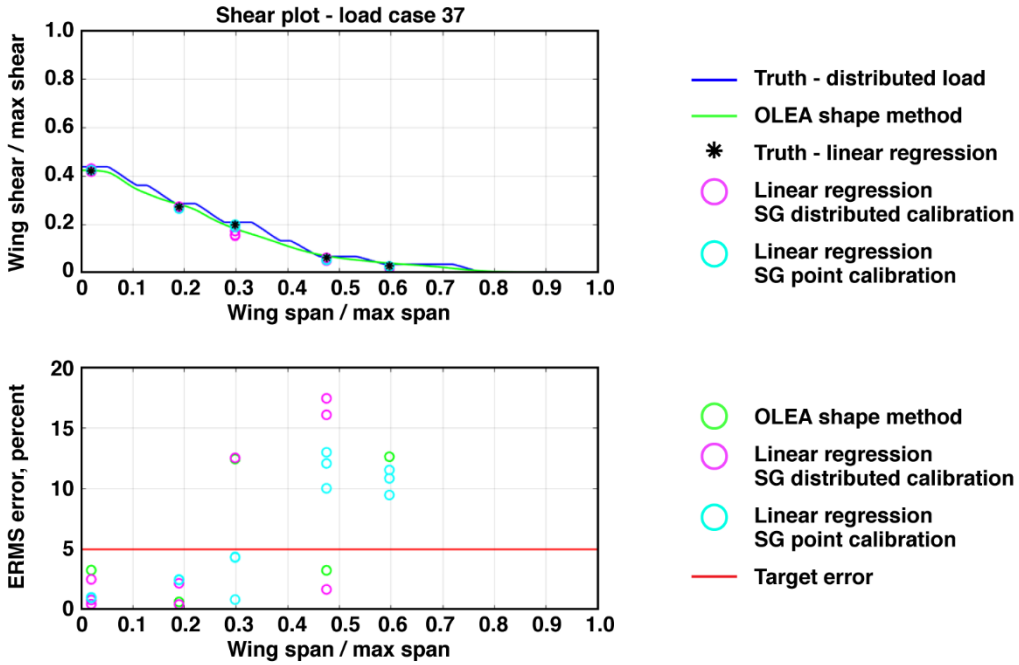

Fig. 24. Load check case 37 results – wing shear.

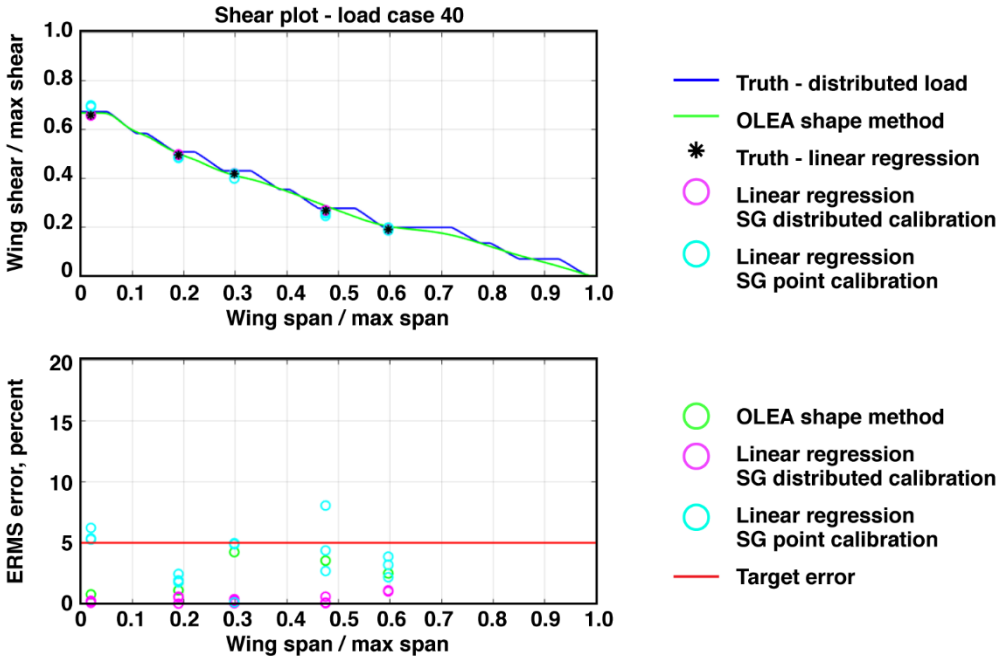

Fig. 25. Load check case 40 results – wing shear.

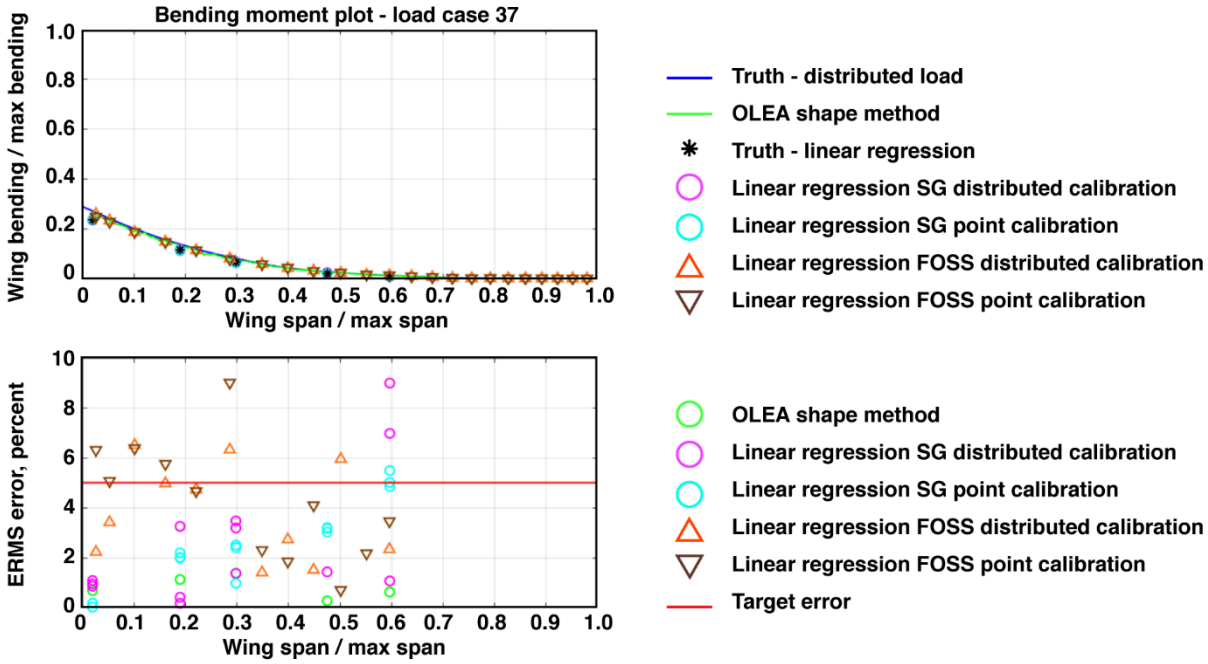

Fig. 26. Load check case 37 results – wing bending.

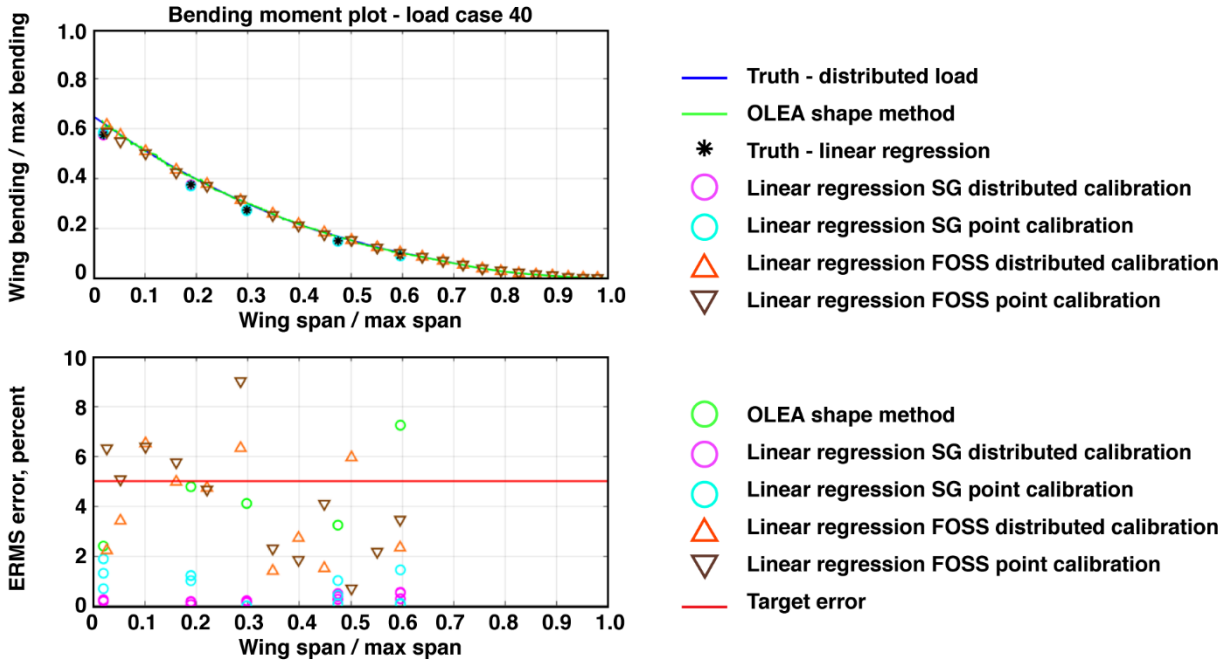

Fig. 27. Load check case 40 results – wing bending.

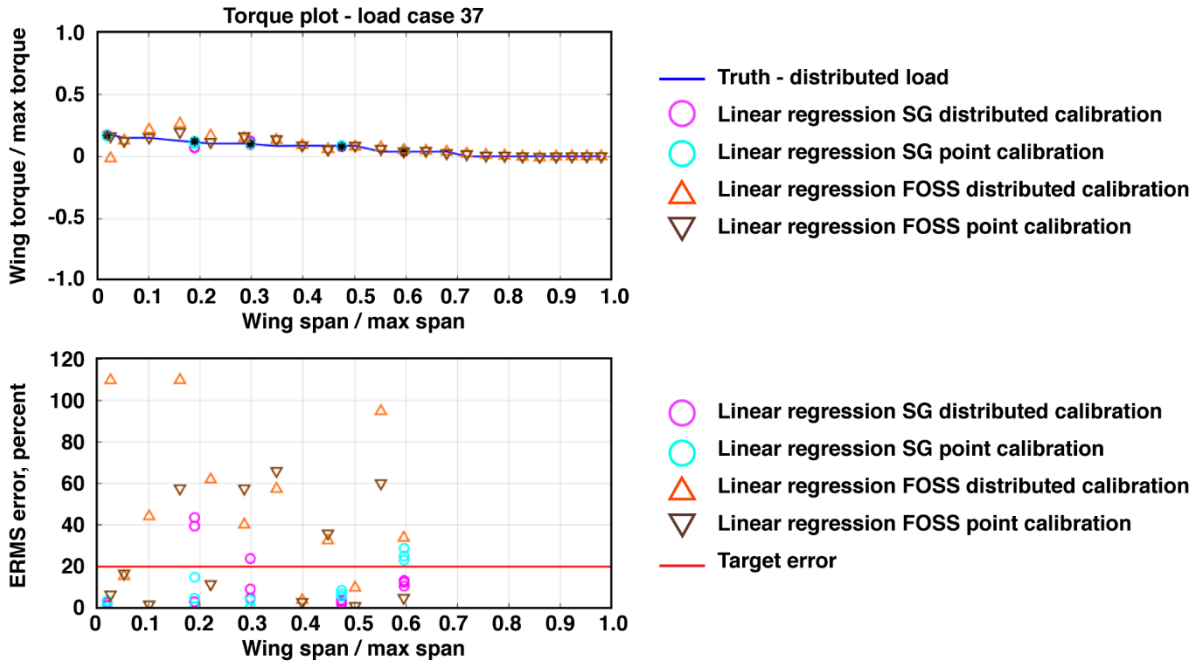

Fig. 28. Load check case 37 results – wing torque.

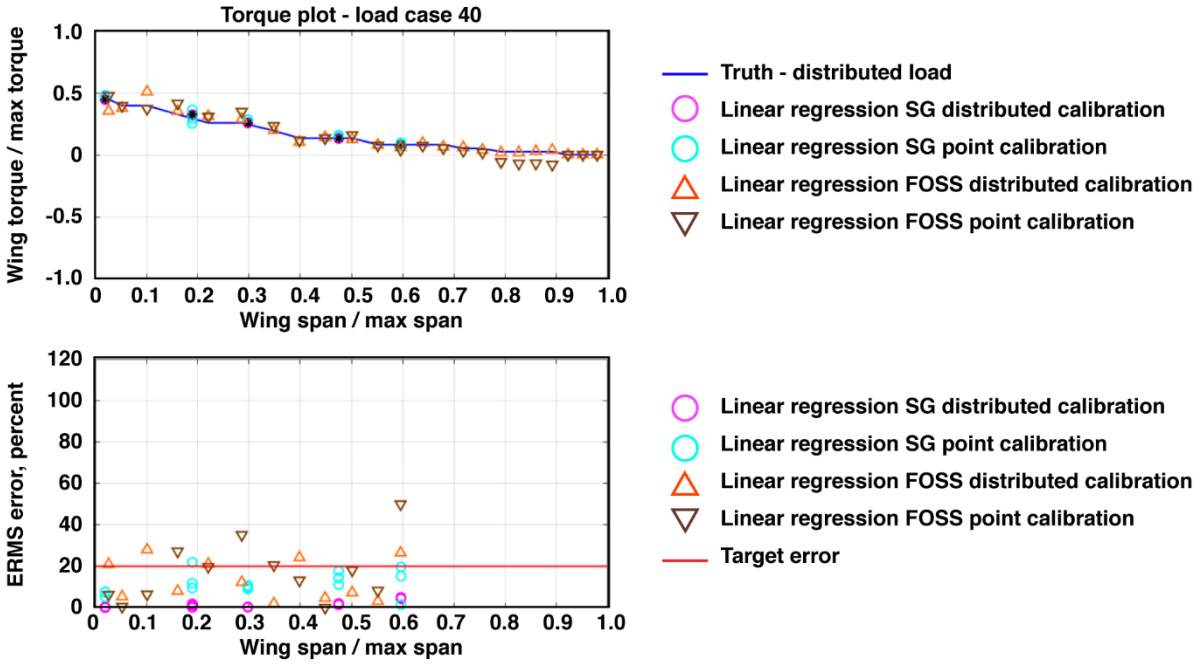

Fig. 29. Load check case 40 results – wing torque.

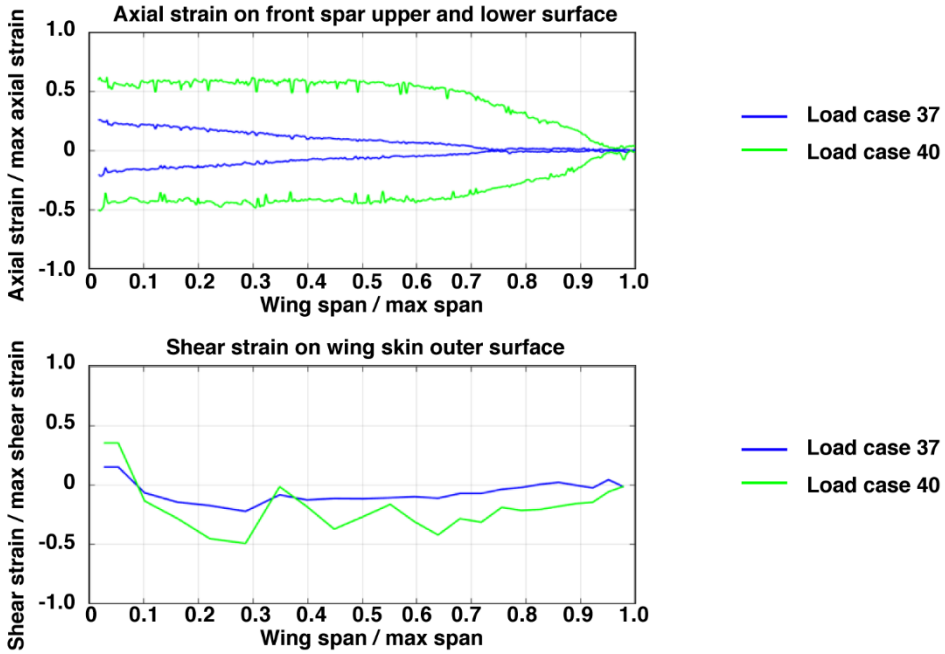

Fig. 30. FOSS strains for load case 37 and 40.

Acknowledgments

The authors gratefully acknowledge the support of Mauricio Rivas from the National Aeronautics and Space Administration Armstrong Flight Research Center in providing funding to support the testing effort. Also Larry Camacho, and Evert Diks from the National Aeronautics and Space Administration Armstrong Flight Research Center in supporting the transfer of the wing to the Flight Loads Lab. Also, the authors acknowledge the help and support from the National Aeronautics and Space Administration Armstrong Flight Research Center Flight Loads Lab, who assisted with the instrumentation installation and load testing.

References

[1] Sims, R., McCrosson, P., Ryan, R., and Rivera, J., "X-29A Aircraft Structural Loads Flight Testing," NASA TM-101715, 1989.

[2] Lokos, W., and Stauf, R., "Strain-Gage Loads Calibration Parametric Study," *24th International Congress of the Aeronautical Sciences*, 2004.

[3] Staszewski, W., Boller, C., and Tomlinson, G.R., *Health Monitoring of Aerospace Structures: Smart Sensor Technologies and Signal Processing*, John Wiley & Sons, Ltd., Chichester, West Sussex, England, 2004.

[4] Miller, E. J., Cruz, J., Lung, S.-F., Kota, S. Ph.D., Ervin, G., and Lu, K.-J. Ph.D., "Evaluation of the Hinge Moment and Normal Force Aerodynamic Loads from a Seamless Adaptive Compliant Trailing Edge Flap in Flight," AIAA 2016-0038, Jan. 2016. doi: 10.2514/6.2016-0038

[5] National Aeronautics and Space Administration, "Experimental Wing Proving New Design Methods," URL: https://www.nasa.gov/centers/armstrong/features/pat_wing.html [retrieved 25 October, 2018].

[6] DeAngelis, V. M.: "Wing Panel Loads and Aileron Hinge Moments Measured in Flight on the F-8 Supercritical Wing Airplane Including Correlations With Wind Tunnel Data," NASA TM X-3098, 1974.

[7] Cruz, J., and Miller, E., "Evaluation of Load Analysis Methods for NASA's GIII Adaptive Compliant Trailing Edge Project," AIAA-2016-0804, Jan. 2016. doi: 10.2514/6.2016-0804

[8] Richards, W. L., Ph.D., Parker, A., Ko, W. L., Ph.D., Piazza, A., and Chan, P. Ph.D., "Application of Fiber Optic Instrumentation," RTO AGARDograph 160, July 2012.

[9] Jenkins, J. M., and DeAngelis, V. M., "A Summary of Numerous Strain-Gage Load Calibrations on Aircraft Wings and Tails in a Technological Format," NASA TM-4804, 1997.

[10] Tesslcr, A., and Spanglcr, J. L., "Inverse FEM for Full-Field Reconstruction of Elastic Deformations in Shear Deformable Plates and Shells," *2nd European Workshop on Structural Health Monitoring*, Munich, Germany, July 7-9, 2004.

[11] Tessler, A., and Spangler, J. L., "A Least-squares Variational Method for Full-Field Reconstruction of Elastic Deformations in Shear-Deformable Plates and Shells," *Computer Methods in Applied Mechanics Engineering*, Vol. 194, No. 2-5, 2005, pp. 327-339. doi:10.1016/j.cma.2004.03.015

[12] Tessler, A., "Structural Analysis Methods for Structural Health Management of Future Aerospace Vehicles," NASA TM-2007-214871, 2007.

[13] Gherlone, M., Cerracchio, P., and Mattone, M., "Shape Sensing Methods: Review and Experimental Comparison on a Wing-Shaped Plate," *Progress in Aerospace Sciences*, Vol. 99, 2018, pp. 14-26. doi: 10.1016/j.paerosci.2018.04.001

[14] Miller, E. J., Manalo, R., and Tessler, A., "Full-Field Reconstruction of Structural Deformations and Loads from Measured Strain Data on a Wing Test Article using the Inverse Finite Element Method," NASA/TM-2016-219407, 2016.

[15] Lizotte, A. M., and Lokos, W. A., "Deflection-Based Structural Loads Estimation from the Active Aeroelastic Wing F/A-18 Aircraft," NASA/TM-2005-212871, 2005.

[16] Allen, M. J., Lizotte, A. M., Dibley, R. P., and Clarke, R., "Loads Model Development and Analysis for the F/A-18 Active Aeroelastic Wing Airplane," NASA/TM-2005-213663, 2005.

[17] Montel, M., and Thielecke, F., "Validation of a Model Based Structural Loads Monitoring System Using the Flight Test Aircraft UW-9 Sprint," AIAA-2015-2237, June 2015. doi: 10.2514/6.2015-2237

[18] Skopinski, T. H, Aiken, W. S. Jr., and Huston, W. B., "Calibration of Strain-Gage Installations in Aircraft Structures for the Measurement of Flight Loads," NACA Report 1178, 1954.

[19] Ko, W. L., Richards, W. L., and Tran, V. T. "Displacement Theories for In-Flight Deformed Shape Predictions of Aerospace Structures," NASA/TP-2007-214612, 2007.

[20] Ko, W. L., and Fleischer, V. T., "Further Development of Ko Displacement Theory for Deformed Shape Predictions of Nonuniform Aerospace Structures," NASA/TP-2009-214643, 2009.

[21] Ko, W. L., Richards, W. L., and Fleischer, V. T., "Applications of Ko Displacement Theory to the Deformed Shape Predictions of the Doubly-Tapered Ikhana Wing," NASA/TP-2009-214652, 2009.

[22] Jutte, C. V., Ko, W. L., Stephens, C. A., Bakalyar, J. A., Richards, W. L. and Parker, A. R. "Deformed Shape Calculation of a Full-Scale Wing Using Fiber Optic Strain Data from a Ground Loads Test," NASA/TP-2011-215975, 2011.

[23] Richards, W. L., and Ko, W. L., *Process for Using Surface Strain Measurements to Obtain Operational Loads for Complex Structures*, U.S. Patent No. 7,715,994, issued, May 11, 2010.

[24] Kreyszig, E., *Advanced Engineering Mathematics*, 9th edition, John Wiley & Sons, New York, 2006.

[25] Pak, C.-G., "Unsteady Aerodynamic Force Sensing from Strain Data," *AIAA Journal of Aircraft*, Vol. 54, No. 4, July–August 2017, pp. 1476-1485. doi: 10.2514/1.C034140

[26] Bakalyar, J., and Jutte, C., "Validation Tests of Fiber Optic Strain-Based Operational Shape and Load Measurements," AIAA-2012-1904, April 2012. doi: 10.2514/6.2012-1904

[27] Lokos, W. A, Miller, E. J., Hudson, L. D., Holguin, A. C., Neufeld, D. C., and Haraguchi, R., "Strain Gage Loads Calibration Testing with Air Bag Support for the Gulfstream III SCRAT Aircraft," AIAA-2015-2020, Jan. 2015. doi: 10.2514/6.2015-2020